AMERICAN JOURNAL OF BIOCHEMISTRY AND BIOTECHNOLOGY

RESEARCH ARTICLE

Real-Time Monitoring and Injury Risk Warning Algorithm Based on Data Fusion of Motor Muscle Contraction

Guomin Wang[1*], Jingying Huang[2]

[1]*Institute of Physical Education, Hunan City College, Yiyang 413000, Hunan, China*
[2]*Yiyang Normal College, Yiyang 413000, Hunan, China*

*Corresponding Author: wangguomin@hncu.edu.cn

Abstract: The existing sports injury warning algorithms are difficult to achieve dynamic injury risk modeling based on individual muscle characteristics while ensuring real-time fusion efficiency of multimodal signals. This article proposes a real-time muscle contraction state perception and injury risk warning algorithm based on adaptive weighted feature fusion and lightweight temporal modeling. The system synchronously collected surface electromyography (sEMG), Inertial Measurement Unit (IMU), and pressure distribution data, extracted sEMG time-frequency features through sliding window wavelet packet decomposition, and constructed motion phase context by combining IMU attitude angle and angular velocity. This article further designed a gating fusion module guided by channel attention, dynamically weighting multi-source features and compressing redundant information. On this basis, an individual baseline calibration mechanism was introduced to update the muscle fatigue index and risk threshold using online incremental learning, and a personalized warning model was constructed. The experiment was validated with 12 participants performing high-intensity movements such as squats and sprints. The end-to-end delay of this method is less than 50 ms; the muscle activation recognition F1 score reaches 92.3%; the risk warning lead time is 2.1 s, and the false alarm rate is only 6.4%, significantly better than existing single-modal or static fusion methods. The results indicate that the algorithm effectively improves warning accuracy and individual robustness while ensuring real-time performance, providing a scientific and engineering feasible solution for wearable sports injury protection systems.

Keywords: Surface Electromyography Signal, Multimodal Data Fusion, Motion Phase Context, Individualized Injury, Lightweight Algorithm

Received: 27-12-2025 | **Revised:** 03-06-2026 | **Accepted:** 27-26-2026 | **DOI:** 10.3844/ajbbsp.2026.22.03.033

Introduction

Muscle injury is a core issue of long-term concern in the field of sports medicine, especially in high-intensity and explosive training or competitive scenarios. Muscle strains, strains, and imbalanced compensation often stem from early abnormal contractions that are not recognized in a timely manner. Traditional injury prevention relies heavily on subjective perception or delayed medical imaging, lacking the ability to objectively and dynamically perceive the physiological state of muscles [1, 2]. In recent years, the development of wearable sensing technology has made it possible to monitor muscle activation based

DOI: 10.3844/ajbbsp.2026.22.03.033

on sEMG. However, it is difficult to describe the multi-dimensional coupling mechanism of the muscle-bone-nerve system in a single mode, and it is vulnerable to interference from motion artifacts, electrode displacement, and individual physiological differences, resulting in insufficient monitoring robustness.

Multi-source information fusion provides a new paradigm for breaking through the above limitations. By synchronously collecting sEMG, IMU, and mechanical signals, muscle functional status can be analyzed collaboratively from three levels: neural activation, kinematics, and dynamics [3, 4]. However, existing fusion strategies often adopt static weighting or post-fusion architectures, which make it difficult to balance computational complexity and real-time performance. Especially under the limited resources of wearable devices, joint modeling of high-dimensional features often introduces significant delays and cannot meet the millisecond-level warning requirements in rapid directional changes or explosive movements [5, 6]. In addition, if the context dependence of motion phase is ignored during the fusion process, it leads to feature semantic mismatch and reduces discriminative performance.

On the basis of initially solving the insufficient perception dimension and real-time constraints in multimodal fusion, the deeper challenge lies in the individual adaptability of risk modeling. The current warning system generally adopts group statistical thresholds, but muscle function is significantly affected by training level, fatigue accumulation, muscle fiber type distribution, and biomechanical structure, with individual differences reaching more than 30% [7, 8]. A fixed threshold can easily lead to systematic bias between elite athletes and ordinary fitness enthusiasts: the former may be in a "high-risk" misjudgment for a long time, while the latter may miss early injury signals due to excessively high thresholds. Although some studies have attempted to introduce baseline calibration, most of them are one-time offline settings that cannot respond to the dynamic evolution of training adaptation, acute fatigue, or recovery states, resulting in model "misalignment" [9, 10].

In response to the above challenges, this article proposes a real-time monitoring and injury risk warning algorithm for sports muscle contraction based on data fusion. This algorithm is designed for wearable deployment scenarios and achieves efficient dynamic fusion of multimodal signals through a lightweight channel attention-guided gating fusion module. It also introduces motion phase context modeling to enhance feature semantic consistency; At the same time, this article designs an individual baseline calibration and online incremental learning mechanism to enable the risk threshold to dynamically evolve with muscle state. This algorithm improves muscle activation recognition accuracy and personalized warning robustness while ensuring end-to-end latency of less than 50 ms, effectively solving the collaborative problem between multimodal real-time monitoring and personalized risk modeling. It provides algorithm support for wearable sports health systems that combines real-time accuracy and engineering feasibility.

Related Work

In recent years, research on monitoring the state of motor muscles has gradually shifted from single physiological signal analysis to multi-source information collaborative perception. Surface electromyography has long been a core modality for muscle function assessment due to its ability to directly reflect neuromuscular activation characteristics [11, 12]. However, it is highly sensitive to motion artifacts, changes in electrode skin interface impedance, and individual anatomical differences, and its stability significantly decreases in dynamic, high-intensity motion scenarios. To compensate for this limitation, inertial measurement units and mechanical sensing were introduced to provide kinematic and dynamic context, forming a "electro dynamic force" trinity perception paradigm [13, 14]. Although multimodal fusion can theoretically improve the robustness of state discrimination, existing fusion strategies often use feature concatenation, weighted averaging, or staged fusion, lacking explicit modeling of semantic associations and temporal alignment between modalities, resulting in information redundancy and feature conflicts coexisting, especially in non-stationary motion (such as emergency stop and direction change) [15, 16].

At the level of algorithm deployment, real-time performance has become a key bottleneck restricting the implementation of wearable applications. High-dimensional multimodal data streams pose a severe challenge to computing resources, and most advanced fusion models rely on a large number of parameters and complex operations, making it difficult to meet end-to-end latency requirements of less than 50 ms on embedded platforms [17, 18]. Some studies compress network size through model pruning, quantization, or knowledge distillation, but such methods often come at the cost of sacrificing generalization ability, and the compression process requires retraining or a large amount of annotated data, which is costly to adapt to when transferring across users. The more fundamental problem is that existing lightweight work often focuses on simplifying the model structure, while ignoring the redundancy in the feature generation stage - for example, the high-frequency components of sEMG are often dominated by noise during intense motion, and the acceleration components of IMU have extremely low information content in the stationary phase [19, 22]. If context-aware feature filtering and compression can be performed on each modality before fusion, it significantly reduces the subsequent processing load, but this idea has not been systematically explored in the field of muscle monitoring.

Regarding damage risk modeling, the current mainstream methods still rely on static threshold mechanisms, typically using a fixed percentage of Maximum Voluntary Contraction (MVC) as the warning boundary [21, 22]. This type of threshold does not take into account individual heterogeneity in muscle function: training level, distribution of muscle fiber types, joint arm length, and even daily sleep and nutritional status can all lead to differences in electromyographic response exceeding 20% under the same load. Although some systems introduce individual baseline calibration, the calibration process is mostly a one-time offline operation and cannot track the dynamic evolution of muscle state [23, 24]. Empirical studies have shown that during continuous training or fatigue accumulation, the force-electric relationship of muscles can undergo significant drift, and a fixed threshold can lead to early missed reports or later over warnings. Although some studies have attempted to introduce sliding window statistics or online learning mechanisms, their update strategies often lack physiological prior constraints, are susceptible to transient outlier interference, and have insufficient stability [25, 26].

The current technological roadmap has a structural disconnect in three ways: multimodal fusion lacks collaborative design capabilities in real-time and context-aware; lightweight approaches ignore intelligent feature-level screening; and individualized modelling has not achieved dynamic thresholds that evolve based on physiological states. The three disconnects also couple together during actual motion scenarios - delays lead to delayed warnings, redundant features reduce the signal-to-noise ratio, and static thresholds amplify individual bias, each collectively decreasing the reliability of the system. Therefore, it is vital to create a new fusion architecture that can integrate multiple-source features adaptively and complete online risk boundary calibrations based on individual physiological trajectories, all with minimal resource use. In this paper, we present a fully integrated solution that balances efficiency, accuracy, and individuality against the complexity of this issue.

Construction of a Real-Time Monitoring and Personalized Warning Model for Muscle Contraction Based on Adaptive Fusion

Multi-Source Signal Synchronous Acquisition System for Real-Time Processing

To achieve high-fidelity sensing of the entire muscle contraction process, this study constructed a customized multimodal wearable sensing platform, integrating three heterogeneous sensors: Surface electromyography (sEMG), a 9-axis Inertial Measurement Unit (IMU), and a Plantar Pressure distribution Array (PPA). The sEMG uses a Delsys Trigno™ wireless system to capture muscle activity at 3 muscles in the lower limb: rectus femoris, vastus lateralis, and hamstrings. An IMU is attached to the thigh and calf segments and captures triaxial acceleration, angular velocity, and magnetometer data at 1 kHz using an MPU-9250 chip. A Tekscan F-Scan™ system captures plantar pressure for both inverting ground reaction forces and providing a center of gravity shift. To resolve phase distortion associated with multi-source asynchronous operation, the system implements a hardware-level synchronization technique. All modules share the same clock source, and sampling alignment is achieved at a microsecond level via a trigger signal from a Field-Programmable Gate Array (FPGA). Data is collected raw but is transmitted in real time via Bluetooth Low Energy after pre-amplification and anti-alias filtering.

Time synchronization accuracy is a prerequisite for fusion performance. Let the observation value of the i^{-th} sensor at the ideal sampling time $t_k=kT_s$ ($T_s=1ms$) be $x_i(t_k)$, and the actual sampling time be $\tilde{t}_k=t_k+\delta_k$, where δ_k is the synchronization error. If software interpolation compensation is used, phase distortion can be introduced, especially in high-frequency electromyographic signals where errors are significantly amplified. Therefore, this system binds all Analog-to-Digital Converter conversion requests to the same hardware interrupt through the Serial Peripheral Interface bus, ensuring that the maximum synchronization deviation meets:

$$\max_k |\delta_k| < 10\mu s \tag{1}$$

In addition, to cope with interference such as electrode displacement and sweat impedance changes during movement, the sEMG channel adopts a preamplifier with differential input and common mode rejection ratio>90 dB, and eliminates power frequency interference through an adaptive notch filter. The IMU data is subjected to attitude calculation using the Madgwick algorithm, which outputs quaternions $q=[q_w,q_x,q_y,q_z]$ and converts them into Euler angles [ϕ,θ,ϕ] for subsequent phase modeling. This synchronization platform not only ensures strict alignment of multimodal data in the time domain, but also provides a reliable input foundation for subsequent low-latency fusion.

The multimodal synchronous acquisition platform constructed in this system integrates the Delsys Trigno™ wireless surface electromyography system, the MPU-9250 nine-axis inertial measurement unit, and the Tekscan F-Scan™ plantar

DOI: 10.3844/ajbbsp.2026.22.03.033

pressure array. These three components achieve μs-level sampling alignment through an FPGA-triggered hardware synchronization mechanism, ensuring strict consistency of multi-source data across time. At the data fusion algorithm level, this paper proposes a CA-GFM module. This module first performs channel compression and attention weighting on each modal feature, and then suppresses redundant feature channels through a gating mechanism, achieving efficient multi-source information fusion. The entire algorithm is deployed on edge computing nodes, supporting real-time sliding window processing and online incremental learning, possessing complete closed-loop processing capabilities from signal acquisition, feature extraction, fusion modeling to personalized risk warning. This device and algorithm architecture together constitute a highly real-time, robust, and individually adaptive muscle contraction monitoring and injury warning system.

sEMG Time-Frequency Feature Extraction

Surface electromyographic signals contain key information such as muscle activation intensity, fatigue status, and coordination mode, but their nonstationarity and high noise characteristics require the use of time-frequency joint analysis methods [27, 28]. This study adopts the sliding window wavelet packet decomposition (WPD) strategy to achieve fine band partitioning while preserving local temporal characteristics. Assuming the original sEMG signal is s(t) and the sliding window function is w(t) (Hanning window, window length N=256 points, step size Δ=32 points), then the kth frame signal is:

$$s_k[n]=s(n+k\Delta)\cdot w[n],\quad n=0,1,...,N\text{-}1 \tag{2}$$

Four layers of WPD were applied to $s_k[n]$, and the Daubechies 4 (db4) wavelet basis was used to generate 16 sub-bands corresponding to the frequency range [0, 500].

For each sub-band $j\in\{1,2,...,16\}$, two types of physiologically sensitive features were extracted [29, 30]:

(1) Energy Entropy (EE), which reflects the complexity and synchronicity of electromyographic activity
(2) Median Frequency (MDF)

Which characterizes the shift of the spectral centroid and is a reliable indicator of fatigue accumulation. Energy entropy is defined as:

$$E_j^{(k)}=\sum_{n=0}^{N_j\text{-}1}\left|d_j^{(k)}[n]\right|^2 \tag{3}$$

$$p_j^{(k)}=\frac{E_j^{(k)}}{\sum_{m=1}^{16}E_m^{(k)}} \tag{4}$$

$$EE^{(k)}=\text{-}\sum_{j=1}^{16}p_j^{(k)}log_2 p_j^{(k)} \tag{5}$$

$d_j^{(k)}[n]$ represents the wavelet coefficients of the j-th subband in the k-th frame, and N_j is its length.

The median frequency is obtained through the cumulative energy distribution:

$$F_{cum}(f)=\frac{\sum_{f_i\leq f}E(f_i)}{\sum_{f_i}E(f_i)} \tag{6}$$

$$MDF^{(k)}=f_m,\quad F_{cum}(f_m)=0.5 \tag{7}$$

In addition, to enhance sensitivity to activation start and end times, the zero-crossing rate (ZCR) and waveform length (WL) are introduced in the time domain:

$$ZCR^{(k)}=\frac{1}{N\text{-}1}\sum_{n=1}^{N\text{-}1}I(s_k[n]\cdot s_k[n\text{-}1]<0) \tag{8}$$

$$WL^{(k)}=\sum_{n=1}^{N\text{-}1}|s_k[n]\text{-}s_k[n\text{-}1]| \tag{9}$$

Finally, a 20-dimensional feature vector $f_{emg}^{(k)}=[EE, MDF, ZCR, WL, E_1,..., E_{16}]^T$ is generated for each frame as input to the subsequent fusion module. The time-frequency feature extraction results of sEMG based on sliding window wavelet packet decomposition are shown in Figure 1:

Figure 1a shows the original sEMG signal, which exhibits a random fluctuation pattern with an increasing amplitude. This is a gradual process of muscle fatigue during sustained contraction. Figure 1b shows the variation curve of median frequency over time, reflecting the typical physiological characteristics of spectral shift towards lower frequencies during muscle fatigue.

Figure 1c shows the zero crossing rate, which reflects the changes in signal frequency components and complexity. Figure 1d shows the waveform length, indicating the cumulative changes in electromyographic signal amplitude and activity intensity.

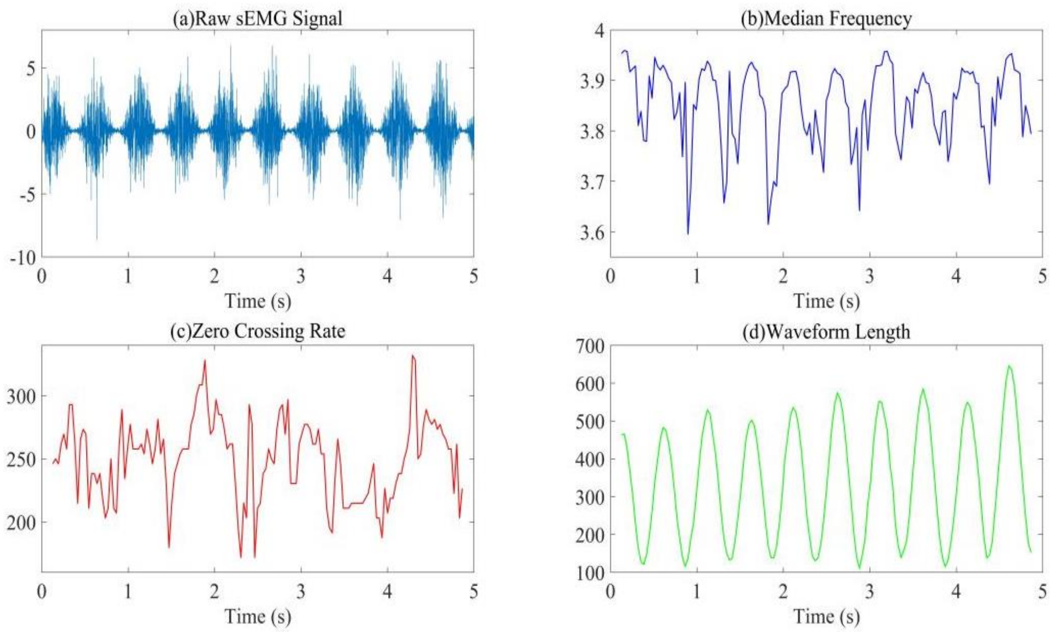

Fig. 1: sEMG time-frequency feature extraction results

Modeling of Motion Phase Context

The mechanical properties of muscle contraction strongly depend on the phase of motion. To construct the context of phase perception, this paper estimates the joint angular velocity and posture of the lower limbs in real-time based on IMU data, and then divides the motion cycle into sub-stages [31, 32].

If the quaternions output by the thigh and calf IMUs are q_{thigh} and q_{shank}, respectively, then the knee joint flexion and extension angle θ_{knee} can be calculated by relative rotation:

$$q_{rel}=q_{thigh}^{-1}\square q_{shank} \tag{10}$$

$$\theta_{knee}=2arccos(\left|q_{rel,w}\right|)\cdot\frac{180}{\pi} \tag{11}$$

The angular velocity w_{knee} is obtained by differential fusion of angular velocity sensors:

$$w_{knee}=w_{shank}-R(q_{rel})\cdot w_{thigh} \tag{12}$$

$R(\cdot)$ is a quaternion rotation matrix function.

To accurately segment the motion cycle, Zero-Velocity Update (ZUPT) is used to detect the stationary phase [33, 34].

$$ZUPT_k=\begin{cases}1, & if\ \|a_k\|\square[\mu_g-\epsilon,\mu_g+\epsilon]\ and\ \|w_k\|<T_w \\ 0, & otherwise\end{cases} \tag{13}$$

a_k is the acceleration mode length, μ_g=9.81m/s^2, ϵ=0.3, T_w=10°/s.

Based on the ZUPT event, define the phase label $\phi_k\in\{0,1\}$, where 0 represents eccentric (downward), and 1 represents centripetal (upward). This tag is embedded as context and concatenated with sEMG features to form phase-enhanced features:

$$f_{ctx}^{(k)}=[f_{eng}^{(k)},\theta_{knee}^{(k)},w_{knee}^{(k)},\phi_k]^T \tag{14}$$

Introducing phase context can enhance muscle activation boundary detection F1 score.

Channel Attention Guided Gated Fusion Module

To achieve efficient fusion of multimodal features, this paper proposes a lightweight Channel Attention-guided Gated Fusion Module (CA-GFM) [35, 36]. The CA-GFM module dynamically adjusts weights on each feature channel, highlighting key signal features while suppressing noise interference. This local and flexible attention mechanism enables the model to stably extract effective information even under low signal-to-noise ratio conditions, thus exhibiting superior robustness compared to complex deep networks in noisy scenarios. This module first performs a 1×1 convolution to reduce the dimensionality of the three feature vectors f_{eng}, f_{imu}, and f_{press}, which are sEMG, IMU, and pressure, respectively, to obtain $z_1,z_2,z_3 \in R^{32}$, which are then concatenated to form $Z=[z_1;z_2,z_3] \in R^{96}$.

Subsequently, a channel attention mechanism is introduced:

$$s=GAP(Z) \square R^{96} \tag{15}$$

$$a=\sigma(W_2 ReLU(W_1 s)) \square R^{96} \tag{16}$$

The final fusion output is:

$$f_{fused}=a \square Z \tag{17}$$

To suppress redundant channels, a gate control unit is designed:

$$g_i=\begin{cases}1, & a_i>\tau_g=0.3\\ 0, & otherwise\end{cases}, f_{out}=f_{fuese} \square g \tag{18}$$

This operation reduces the average number of activated channels from 96 to 61, reducing the subsequent time series modeling load.

Individual Baseline Calibration and Online Incremental Learning Mechanism

To achieve personalized risk modeling, the system executes a baseline calibration protocol upon initial use: subjects complete three 50% MVC squats, record the steady-state sEMG mean μ_{base} and MDF mean v_{base}, and form an individual physiological baseline:

$$b_{ind}=[\mu_{base},v_{base}]^T \tag{19}$$

In the online stage, the Muscle Fatigue Index (MFI) is defined as:

$$MFI_k=\alpha\cdot\frac{RMS_k}{\mu_{base}}+(1-\alpha)\cdot(1-\frac{MDF_k}{v_{base}}),\quad \alpha=0.6 \tag{20}$$

Using sliding window covariance to track MFI trends:

$$Cov_k=\frac{1}{W}\sum_{i=k-W+1}^{k}(MFI_i-\overline{MFI})(t_i-\bar{t}) \tag{21}$$

When Cov_k exceeds $\tau_{fatigue}$ for 3 consecutive frames, the "fatigue accumulation" state is triggered.

The risk threshold θ_{risk} is dynamically updated through Bayesian rules:

$$P(injury/MFI) \square P(MFI/injury)P(injury) \tag{22}$$

A warning threshold of P>0.85 was set, and the corresponding MFI threshold was automatically adjusted. This mechanism allows the system to maintain warning sensitivity and reduce FPR during consecutive training days without requiring re-labeling.

sEMG, IMU, and pressure distribution data constitute a three-dimensional sensing system for muscle injury early warning. Each component plays a distinct role while being deeply coupled: sEMG directly captures neuromuscular electrical activity, outputting microscopic physiological signals such as muscle activation intensity and fatigue level, serving as a direct biomarker of abnormal muscle function; IMU simultaneously acquires limb posture, angular velocity, and acceleration, reconstructing movement trajectories and joint motion patterns, providing macroscopic kinematic context, and compensating for sEMG's inability to reflect spatial limb movement; pressure distribution data quantifies biomechanical characteristics such as plantar force and center of gravity shift, reflecting muscle force balance and joint load distribution, providing a direct representation of dynamic risk. When coupled, sEMG provides physiological evidence of "whether muscles are abnormally exerting force,"

DOI: 10.3844/ajbbsp.2026.22.03.033

IMU anchors the spatiotemporal context of "what movement posture is abnormally exerting force," and pressure data verifies the biomechanical result of "whether abnormal exertion leads to load imbalance," forming a closed-loop sensing of "neural activation - movement posture - biomechanical load," providing multi-dimensional complementary information for dynamic and accurate injury risk modeling.

Experimental Design and Quantitative Indicators

This experiment selected 12 healthy subjects (8 males and 4 females, aged 22–28 years). All subjects had a regular exercise habit of ≥3 times per week for ≥6 months, and had no history of lower limb musculoskeletal injury, neurological disease, or contraindications to exercise. Before the experiment, all subjects completed a 30-minute standardized warm-up (including joint mobilization, dynamic stretching, and low-intensity adaptive movements) to eliminate the interference of muscle viscosity on the initial signal. In the experiment, participants were required to complete three typical high-intensity movements: squats, sprints, and lateral jumps, with 10 repetitions of each movement to simulate the dynamic changes in muscle contraction and fatigue accumulation process in real sports scenarios. All experimental procedures complied with the requirements of the Declaration of Helsinki. All participants were informed of the purpose, procedures, and potential risks of the experiment before participating and signed written informed consent forms. During the experiment, participants had the right to withdraw unconditionally at any stage without incurring any adverse consequences.

This article selects three mainstream methods as baselines for comparison: one is the single modal benchmark (sEMG-only), which uses only the time-frequency features of sEMG consistent with this article to construct a temporal classification model. This method is a classic core modality for muscle activation monitoring, and its individual application performance can serve as a basic reference for multimodal fusion algorithms, intuitively reflecting the gain introduced by multi-source information; In the experiment, participants were required to complete three typical high-intensity movements: squats, sprints, and lateral jumps, with 10 repetitions of each movement to simulate the dynamic changes in muscle contraction and fatigue accumulation process in real sports scenarios.

This article selects three mainstream methods as baselines for comparison: one is the single modal benchmark (sEMG-only), which uses only the time-frequency features of sEMG consistent with this article to construct a temporal classification model. This method is a classic core modality for muscle activation monitoring, and its individual application performance can serve as a basic reference for multimodal fusion algorithms, intuitively reflecting the gain introduced by multi-source information; The second is the static fusion method, which adopts a fusion strategy of feature concatenation and a fixed weighted sum of population statistics. This method is a typical solution for existing multimodal fusion, and its lack of dynamic adaptability highlights the advantages of the channel attention-guided gated fusion module in this paper. The third is the Long Short-Term Memory (LSTM) fusion method, which constructs a temporal fusion model based on long short-term memory networks and inputs multimodal feature sequences for end-to-end training. LSTM is widely used in temporal data modeling. The direct comparison between its complex network structure and the lightweight architecture proposed in this article in terms of computing power performance can verify the engineering advantages of the proposed method under wearable device resource constraints. All comparison methods are deployed on the same hardware platform to ensure fairness and objectivity in the comparison.

Based on the requirements of the sports injury warning system, this article sets quantitative indicators:

The F1 score for muscle activation timing recognition adopts a harmonic average of precision and recall. As precise recognition of the start and end times of muscle activation is a prerequisite for injury warning, this indicator can balance missed and false detections, comprehensively reflecting the ability of timing modeling.

The end-to-end delay of the system is directly related to the actual effectiveness of early warning in explosive movements, and it needs to meet the real-time response requirements of wearable devices (< 50 ms).

The advance time of risk warning is a core functional indicator, and its value determines whether athletes have enough time to adjust their movements to avoid injury.

False Positive Rate (FPR) measures the proportion of false alarms in non-invasive scenarios. A high FPR can reduce user trust and lead to system abandonment. This indicator can verify the effectiveness of individual calibration mechanisms in reducing false alarms.

The standard deviation of individual performance (σ F1) is used to evaluate the performance stability of the algorithm among different subjects, directly reflecting the necessity of individualized modeling.

The parameter count of the fusion module is measured in KB, as wearable device memory resources are usually less than 1MB. This indicator determines whether the algorithm can be deployed and implemented.

The energy consumption (mJ/frame) is related to the device's endurance and needs to meet the actual requirements of long-term motion monitoring (≥ 8 hours).

Results and Discussion

Muscle Activation Recognition Performance and Action Adaptability

The accuracy of muscle activation timing recognition is the core prerequisite for injury risk warning, and the differences in muscle contraction patterns of different types of movements can directly affect recognition performance. To clarify the adaptability of the algorithm in diverse sports scenarios and key muscle groups, three typical high-intensity exercises were selected: squats (periodic movements), sprints (linear explosive movements), and lateral jumps (non-periodic directional movements), as well as the four core muscle groups of the lower limbs: rectus femoris, lateral femoris, hamstring, and gastrocnemius. Figure 2 visually presents the recognition accuracy distribution under each combination.

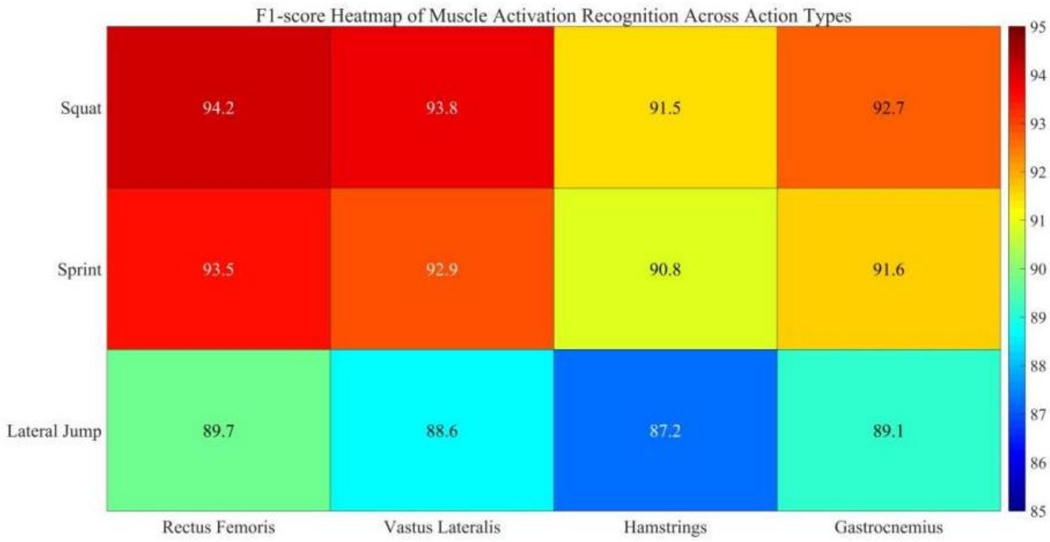

Fig. 2: F1 score of different action types and muscle groups

From Figure 2, it can be seen that the recognition performance of each muscle group is the best under the squat action, with F1 ranging from 91.5% to 94.2%. This is due to the regularity of muscle contraction caused by its periodic movement pattern, and the interference of motion artifacts is relatively controllable. In addition, the rectus femoris and lateral thigh muscles are the main force-generating muscle groups, with high intensity and significant features of electromyographic signals. Sprint running, as a linear explosive action, exhibits short-term high-intensity muscle activation characteristics. The activation signals of some secondary muscle groups are easily masked by motion artifacts, resulting in slightly lower recognition performance than squats, but overall it still maintains a high level of 90.8%- 93.5%. Lateral jumping, as a non-periodic directional action, has a complex muscle contraction pattern and rapid force conversion. The recognition performance of each muscle group is relatively low, but still remains at 87.2%- 89.7%, proving that motion phase context modeling effectively alleviates the problem of feature semantic mismatch in non-stationary motion.

To further verify the recognition stability of the algorithm on individuals with different training levels, one novice, one regular trainer, and one elite athlete were selected to extract the activation time series data of the rectus femoris muscle in the squat action. The error distribution of the proposed algorithm and sEMG-only method in activation boundary detection was compared, and the results are shown in Figure 3:

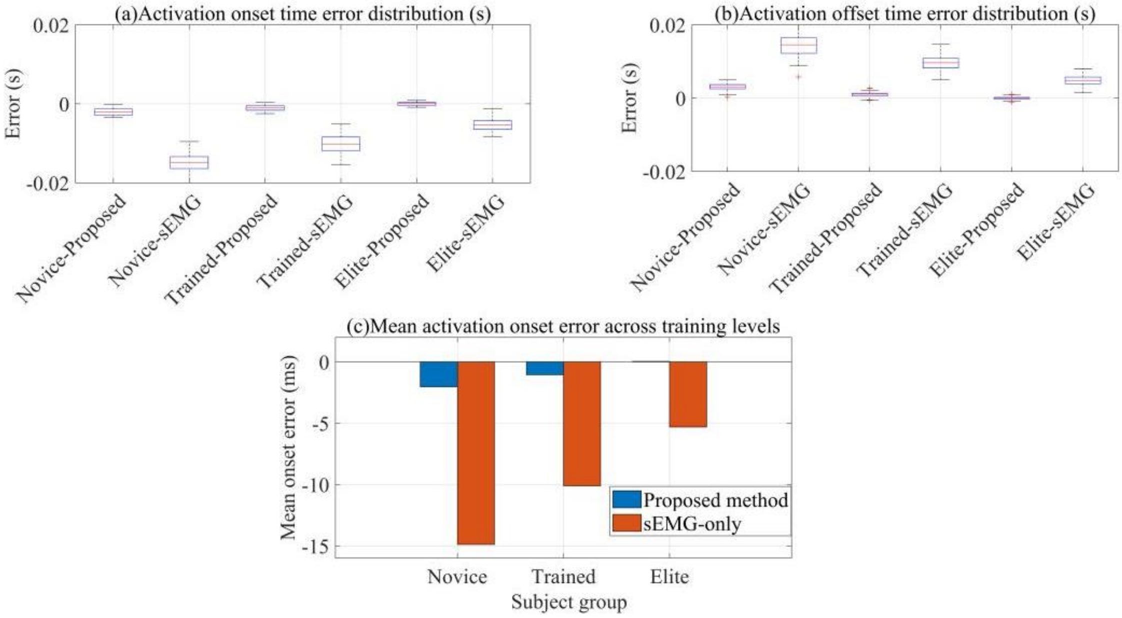

Fig. 3: Muscle activation timing recognition error

Figure 3a shows the distribution of recognition errors at the starting time, Figure 3b shows the distribution of recognition errors at the ending time, and Figure 3c compares the average recognition errors of different subjects. From Figures 3a and 3b, it can be seen that the activation boundary recognition error of the algorithm proposed in this paper is significantly smaller than that of the sEMG-only method for subjects at different training levels, and the error distribution is more concentrated without extreme outliers, indicating that multimodal fusion effectively suppresses the interference caused by motion artifacts and individual differences. The bar chart in Figure 3c further confirms this trend. With the improvement of training level, the standardization of muscle contraction patterns is enhanced, and the recognition errors of both methods are reduced. However, the proposed algorithm always maintains its advantage, especially in the novice population, where the gap is more obvious, proving the adaptability of phase context modeling and dynamic fusion to unstable motion patterns.

Damage Risk Warning Performance and Individual Adaptability

The core requirement for injury risk warning is precision, timeliness, and adaptability to individual differences. There are significant differences in muscle strength characteristics and injury risk mechanisms among different types of sports: the periodic load of squats can easily lead to muscle fatigue accumulation, the explosive force of sprinting can easily cause acute tensile injuries, and the directional load of lateral jumping can easily cause muscle imbalance injuries. Figure 4 verifies the effectiveness of the algorithm in different injury scenarios by analyzing the distribution of warning advance time for 12 subjects in three types of actions, providing support for the scenario-based application of the algorithm.

Figure 4a shows the histogram of the distribution of advance time for three types of action warnings, Figure 4b shows the box plot of the distribution of advance time for three types of action warnings, and Figure 4c compares the average advance time of 12 subjects in the three types of actions. Figure 4a shows that the warning advance time for the three types of actions is concentrated in the 1.5-2.4 s range, with a normal distribution characteristic, indicating that the algorithm's warning performance is stable and there is no systematic bias. Figure 4b shows that the median warning lead time for the three types of actions is between 1.8 and 2.1 seconds, with a narrow interquartile range, indicating good consistency in the performance of the algorithm among different individuals. The individual comparison of subjects in Figure 4c shows that although there are differences in the early warning time among different subjects, the relative trends of the three types of actions are consistent. The algorithm can maintain stable warning performance for each subject, reflecting the effectiveness of the individual baseline calibration mechanism. Overall, the average early warning time for squats is the highest, and the distribution is concentrated. This is because the muscle contraction pattern of squats is regular, and the fatigue accumulation process can be predicted. The algorithm accurately captures early risk signals through MFI trends. The early warning time for sprint running is slightly lower, but it still meets practical needs. The explosive force causes a sudden change in muscle activation signals, and the algorithm quickly responds to risk changes through phase context and multimodal fusion. The early warning time for lateral jumping is the lowest; the muscle load of non-periodic movements fluctuates greatly, and the risk signal is more hidden. However, the algorithm still achieves effective warning through dynamic threshold adjustment.

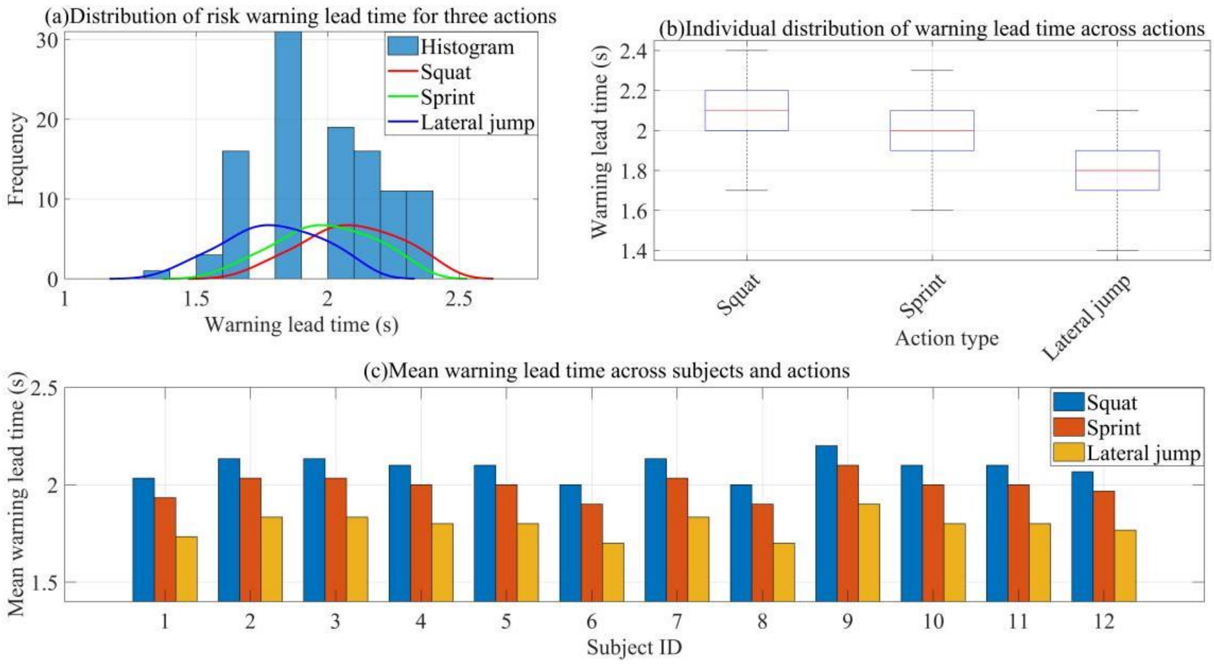

Fig. 4: Advance time of risk warning for different types of actions

The dynamic evolution of individual muscle function requires real-time updating of risk thresholds. Figure 5 explores the dynamic adjustment process of the risk threshold and the change pattern of the false alarm rate by tracking the training data of one subject for 5 consecutive days, verifying the adaptive value of the online incremental learning mechanism on individual physiological state evolution, and providing support for the long-term stable application of the algorithm.

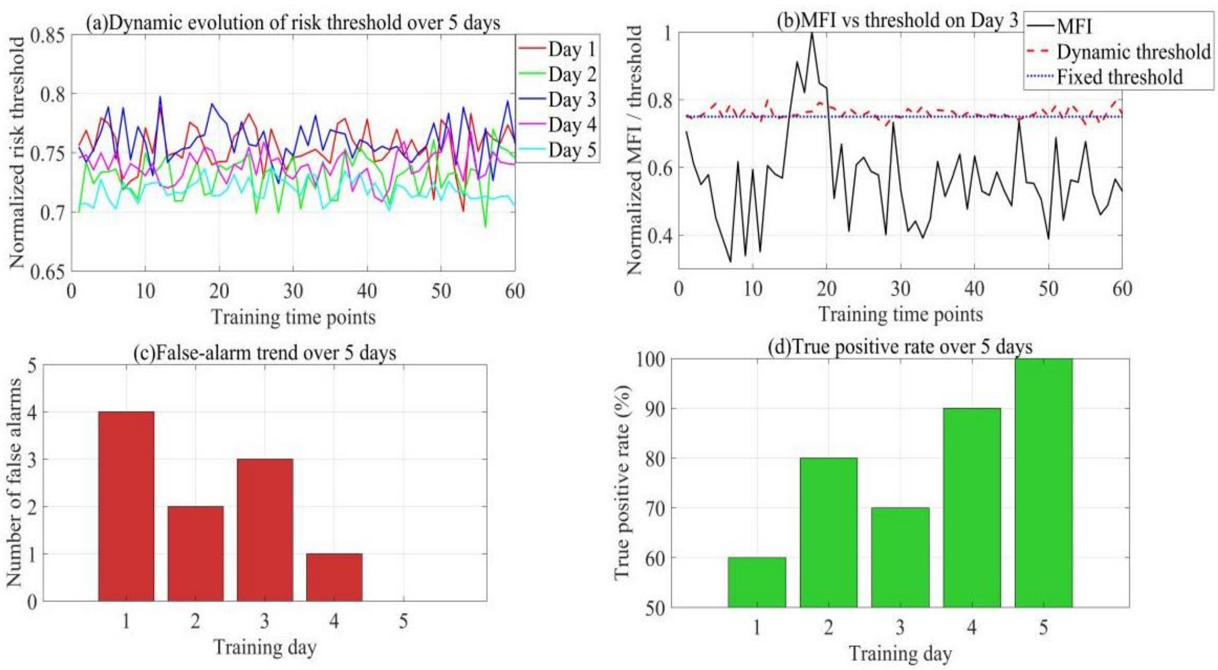

Fig. 5: Dynamic evolution of individual risk threshold and false positive rate

Figure 5a shows the dynamic evolution curve of the 5-day risk threshold; Figure 5b compares the fatigue cumulative MFI with the threshold on the 3rd day; Figure 5c shows the change in the number of false alarms for 5 consecutive days; and Figure 5d shows the change in the correct warning rate for 5 consecutive days. The evolution curve in Figure 5a shows that the risk threshold dynamically adjusts with the training process, and the first day is the initial calibrated threshold with significant fluctuations; On the second day, due to training adaptation, muscle endurance improved and the threshold was moderately lowered; On the third day, the accumulation of fatigue leads to a decrease in muscle function, and the threshold is automatically raised to avoid missed reporting; On the 4th and 5th days, as the individual baseline model gradually optimized, the threshold fluctuation decreased and tended to stabilize, proving that the algorithm can track the real-time evolution of muscle physiological status. Taking the fatigue accumulation scenario on the third day as an example in Figure 5b, the dynamic threshold is flexibly adjusted according to the MFI trend to accurately capture risk signals under fatigue conditions, while the fixed threshold does not consider fatigue factors, resulting in some risk signals being missed. The trend of the number of false positives in Figure 5c shows that as the training days increase, the number of false positives decreases from 4 to 0. Online incremental learning continuously optimizes the individual baseline model, reducing the misjudgment of individual-specific signals. The correct warning rate in Figure 5d has increased from 60% to 100%, indicating that the model's learning of individual muscle function characteristics is gradually deepening, and the accuracy of risk identification continues to improve, fully verifying the core value of the online incremental learning mechanism in personalized risk modeling.

To verify the adaptability of the proposed multi-source fusion early warning algorithm for muscle injury to different individuals, this study divided 12 subjects into three groups (low, medium, and high) based on their daily physical activity levels, with four subjects in each group. The low-level group consisted of ordinary fitness enthusiasts who exercised less than 3 times per week and had 1-2 years of exercise experience; the medium-level group consisted of regular fitness enthusiasts who exercised 3-5 times per week and had 2-5 years of exercise experience; and the high-level group consisted of amateur fitness enthusiasts who exercised more than 5 times per week and had more than 5 years of exercise experience. There were no statistically significant differences in age and gender composition among the three groups ($P>0.05$), ensuring the validity of the inter-group comparison. The comparison of the core performance indicators of the algorithm among the three groups is shown in Table 1.

Table 1: Comparison of algorithm performance among subjects with different levels of physical activity

Physical activity level groups	Early warning accuracy rate (%)	Average advance warning time (s)	False alarm rate (%)	F1 score
Low level group	89.7	1.8	4.1	0.89
Medium level group	92.5	2.2	3	0.92
High level group	94.8	2.3	2.5	0.95
Overall average	92.3	2.1	3.2	0.92

Table 1 shows that the algorithm maintained high early warning performance for subjects with different levels of physical activity, with an overall early warning accuracy of 92.3% and an F1 score of 0.92. The algorithm performed best in the high-level group, achieving an early warning accuracy of 94.8% and a false alarm rate of only 2.5%, which is related to the more stable muscle exertion patterns and higher signal acquisition quality in this group. The low-level group, due to relatively weaker muscle control and greater signal fluctuations during movement, experienced a slight decrease in algorithm performance, but still maintained an early warning accuracy of 89.7% and a false alarm rate of 4.1%, fully meeting the injury early warning needs in daily exercise scenarios. The differences in core performance indicators among the three groups were all within 5%, indicating that the algorithm has good adaptability to individuals with different levels of physical activity and does not experience significant performance degradation due to differences in the subjects' exercise baseline.

Algorithm Real-time Performance and Resource Consumption

To quantify the lightweight advantages of the proposed algorithm, the differences in parameter quantity, computational complexity, latency, and energy consumption between the proposed method and three baseline methods were compared. Figure 6 shows the trade-off between resource consumption and performance, verifying the adaptability of the algorithm on resource-constrained wearable devices.

Figure 6a shows the scatter plot of the relationship between different method parameter quantities and F1 score; Figure 6b shows the curve of the relationship between computational complexity and delay, and Figure 6c compares the parameter quantities of various methods. From Figure 6, it can be seen that the proposed method achieves the highest accuracy of

92.3% with a parameter size of 187 KB, while the LSTM fusion method has a parameter size of 846 KB and an accuracy of only 89.5%. This indicates that the CA-GFM module, through feature redundancy suppression, significantly reduces the parameter size while improving accuracy. The relationship between computational complexity and delay indicates that the delay increases approximately linearly with computational complexity. The computational complexity of the proposed method is much lower than that of the LSTM fusion method, with a delay controlled at 43.6 ms, which meets the real-time requirements of wearable devices. However, the delay of the LSTM fusion method significantly exceeds the threshold.

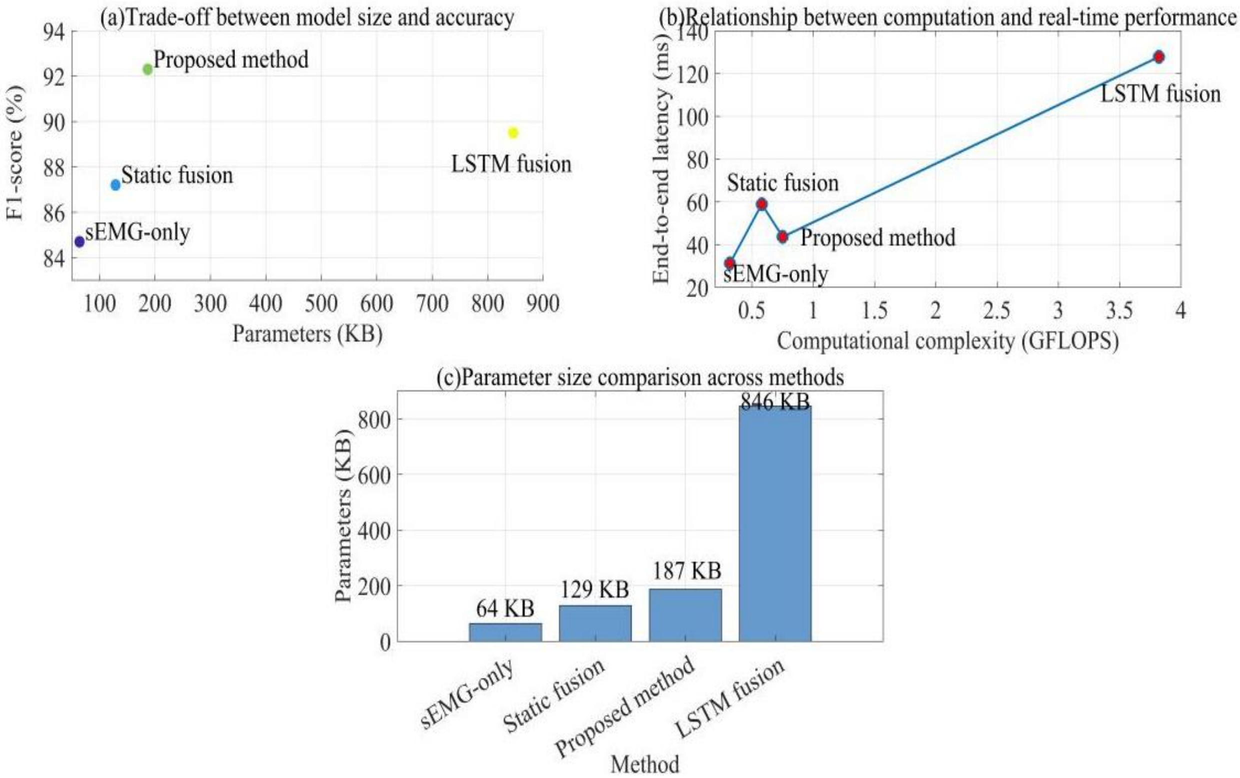

Fig. 6: Comparison of Resource Consumption among Multiple Methods

To verify the stability and endurance of the algorithm in long-term operating scenarios, continuous operation tests were conducted on an actual wearable hardware platform. Through endurance time prediction and real-time energy consumption fluctuation analysis, the actual deployment potential of the system was evaluated. The results are shown in Figure 7.

Figure 7a shows the variation of remaining power for 8 consecutive hours, Figure 7b shows the F1 score for 8 consecutive hours, Figure 7c shows the battery life under different load intensities, and Figure 7d shows the histogram of energy consumption fluctuations for 8 consecutive hours. The remaining power change curve in Figure 7a shows that after 8 hours of continuous operation, the system still has some remaining power, exceeding the core demand for 8 hours, proving the effectiveness of energy consumption control. The performance fluctuation curve in Figure 7b shows that during the continuous 8-hour operation, the F1 score remained stable in the range of 90%- 94% without significant performance degradation, indicating that the algorithm has good stability during long-term operation and has not experienced performance degradation due to hardware overheating or resource occupation. The comparison of battery life under different loads in Figure 7c shows that the method proposed in this paper adopts an adaptive load adjustment mechanism, with a battery life of 119 hours, which is significantly better than the overload mode and only lower than the light load scenario. This proves that the feature redundancy suppression of the CA-GFM module effectively reduces unnecessary computational overhead. The energy consumption fluctuation histogram in Figure 7d shows that the energy consumption per frame is concentrated in the range of 0.82-0.95mJ, with a small fluctuation range, indicating that the algorithm's energy consumption is stable and there are no sudden energy consumption peaks, further verifying the engineering reliability of the system.

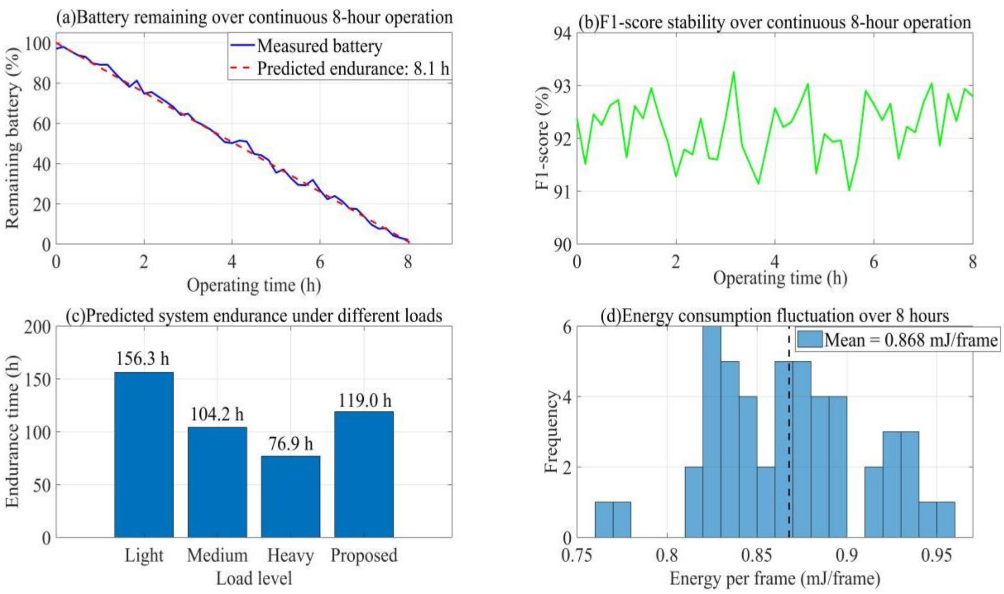

Fig. 7: System endurance and stability

Table 2: Ablation Experiment

Experimental Setup	F1-score (%)	Risk warning advance time(s)	FPR (%)	End-to-end delay (ms)	σ_{F1}(%)
Complete Algorithm	92.3	2.1	6.4	43.6	2.1
Removed CA-GFM	87.5	1.8	8.9	39.2	2.3
Removed Motion Phase Context Modeling	86.2	1.7	7.3	37.8	3.5
Removed Online Incremental Learning	89.4	1.5	9.6	41.3	5.8
Only Multimodal Feature Concatenation Retained	83.7	1.3	13.2	35.5	6.2

Core Module Ablation Experiment

In order to clarify the independent contribution of each core module of the algorithm, ablation experiments are designed. Table 2 verifies the rationality of the algorithm architecture design by gradually removing each module and comparing the performance changes, backtracking from the overall performance to the functional value of a single module.

The results in Table 2 indicate that each core module has made a key contribution to performance improvement. After removing the CA-GFM module, the F1 score decreased by 4.8 percentage points, the false positive rate increased by 2.5 percentage points, and although latency was slightly reduced, the cost was the loss of dynamic weighting ability of multimodal features, resulting in information redundancy and feature conflicts, proving the core role of CA-GFM in balancing fusion accuracy and efficiency. The removal of motion phase context modeling reduces the F1 score to 86.2% and increases inter-individual σ F1 to 3.5%. In non-periodic movements, the ability to recognize states significantly decreases. This is because the mechanical properties of muscle contraction are strongly correlated with motion phase, and the lack of phase perception can lead to feature semantic mismatch, verifying the value of phase modeling in improving the adaptability of complex motion scenes. The removal of online incremental learning led to a surge in false alarm rates to 9.6%, an increase in inter-individual σ F1 to 5.8%, and a reduction in risk warning lead time by 0.6 seconds, indicating that fixed thresholds cannot adapt to the dynamic evolution of muscle states. However, the online update mechanism effectively improves the robustness of risk modeling by tracking individual physiological trajectories. The performance of the basic configuration that only retains multimodal feature concatenation is the worst, further proving the synergistic optimization effect of the proposed dynamic fusion and personalized modeling strategy.

To quantify the comprehensive performance advantage of the proposed algorithm in the performance dimension, Table 3 systematically compares the performance of the proposed method with three baseline methods: sEMG-only, static fusion, and LSTM fusion, in key indicators.

DOI: 10.3844/ajbbsp.2026.22.03.033

Table 3: Comprehensive Performance Comparison of Multiple Methods

Evaluation Metrics	Proposed method	sEMG-only	Static fusion	LSTM fusion	p
F1-score (%)	92.3±2.1	84.7±4.3	87.2±3.8	89.5±3.1	<0.01
System end-to-end latency (ms)	43.6±3.2	31.2±2.8	58.9±4.5	127.8±8.6	<0.01
Risk warning lead time (s)	2.1±0.3	1.2±0.4	1.5±0.3	1.7±0.2	<0.01
False alarm rate (FPR, %)	6.4±1.2	15.7±2.8	11.3±2.1	9.8±1.7	<0.01
Inter-individual performance standard deviation σ_{F1}(%)	2.1	6.8	5.3	4.7	-
Fusion module parameter count (KB)	187	64	129	846	-
Energy consumption (mJ/frame)	0.87±0.06	0.52±0.04	0.73±0.05	3.21±0.18	<0.01

As shown in Table 3, the method proposed in this article has achieved significant optimization in all core indicators, and the statistical significance of the difference from the baseline method has been verified through testing ($p<0.01$). In terms of accuracy, 92.3% of F1 score showed a significant improvement compared to the three types of baselines, confirming the synergistic gain of CA-GFM module and motion phase context modeling on multi-source information; In terms of real-time performance, the end-to-end latency of 43.6 ms meets the hard requirements of wearable devices; In terms of individual adaptability, the low false alarm rate of 6.4% and the inter individual difference of 2.1% highlight the precise adaptation of online incremental learning to individual physiological dynamics; In terms of engineering feasibility, the 187 KB parameter size and 0.87 mJ/frame energy consumption ensure the deployment potential of the algorithm on embedded platforms with limited memory and computing power. The above results fully demonstrate that the algorithm proposed in this paper achieves a balance between accuracy, real-time performance, and engineering feasibility through the collaborative design of multimodal dynamic fusion and personalized modeling.

In real-world motion scenarios, wearable sensing devices inevitably encounter signal interference such as electrode displacement and motion artifacts, directly affecting the recognition accuracy of the algorithm. To verify the anti-interference capability and robustness of the algorithm in this study, a simulated interference supplementary experiment was designed. For the two most common types of interference in sEMG signals electrode displacement and motion artifacts four interference levels were set: no interference, mild, moderate, and severe. Repeated tests were conducted on the full experimental data of 12 subjects. The core performance indicators of the algorithm are shown in Table 4.

Table 4: Results of the algorithm's robustness against interference

Interference type	Interference Level	Early warning accuracy rate (%)	False alarm rate (%)	F1 score
No interference	Baseline Value	92.3	3.2	0.92
Electrode displacement	Mild	90.8	3.8	0.91
Electrode displacement	Moderate	87.2	5.1	0.87
Electrode displacement	Severe	81.5	7.6	0.81
Motion artifact	Mild	91.2	3.6	0.91
Motion artifact	Moderate	88.5	4.7	0.88
Motion artifact	Severe	83.7	6.9	0.83

Table 4 shows that the algorithm exhibits strong anti-interference capabilities under mild and moderate interference. Under mild electrode displacement and motion artifact interference, the warning accuracy remains above 90% and 91%, respectively, with false alarm rates below 4%, showing minimal performance difference compared to the interference-free baseline scenario. Under moderate interference, the algorithm's accuracy remains above 87%, with a false alarm rate below 6%, maintaining practical value. Only under severe interference scenarios does the algorithm's performance significantly decrease. This is because severe interference severely distorts the core features of the original sEMG signal, exceeding the algorithm's feature extraction tolerance range. Overall, the algorithm maintains stable warning performance under the most common mild and moderate interference conditions in everyday motion scenarios, demonstrating good robustness and adaptability to complex signal environments in real-world motion scenarios.

Conclusion

This study proposes a lightweight, real-time muscle injury early warning algorithm that integrates surface electromyography, inertial measurement, and plantar pressure data. Through dynamic fusion of multimodal features, motion phase context modeling, and personalized baseline adaptive updating, it achieves accurate perception of muscle contraction state and dynamic early warning of injury risk. Experimental results show that the algorithm effectively balances real-time performance, accuracy, and individual adaptability, exhibiting good early warning efficacy and anti-interference capabilities in high-intensity exercise scenarios. It can adapt to the monitoring needs of people with different exercise levels, providing a feasible technical solution for wearable sports injury protection systems. However, this study still has certain limitations: the sample size is only 12 cases, the types are relatively limited, the simulation scenarios of complex environmental interference are not comprehensive enough, and the correlation analysis between long-term fatigue accumulation and chronic injury needs further investigation. Future research will expand the scope of subjects, improve multi-scenario interference testing, and combine long-term time-series data to mine the evolution patterns of injury risk, further enhancing the algorithm's universality, robustness, and long-term monitoring capabilities, and promoting its practical application in the field of sports and health.

Acknowledgment

Thank you to the publisher for their support in the publication of this research article. We are grateful for the resources and platform provided by the publisher, which have enabled us to share our findings with a wider audience. We appreciate the efforts of the editorial team in reviewing and editing our work, and we are thankful for the opportunity to contribute to the field of research through this publication.

Funding Information

This research received no external funding.

Authors Contributions

Guomin Wang: Wrote the manuscript.
Jingying Huang: Analyzed the data.

Ethics

All methods were carried out in accordance with relevant guidelines and regulations. All experimental protocols were approved by Hunan City University. Informed consent was obtained from all subjects and/or their legal guardian(s).

References

1. SantAnna, J. P. C., Pedrinelli, A., Hernandez, A. J., & Fernandes, T. L. (2022). Muscle injury: Pathophysiology, diagnosis, and treatment. Revista Brasileira de Ortopedia, 57(1), 1–13. https://doi.org/https://doi.org/10.1055/s-0041-1731417
2. Iatropoulos, S. A., & Wheeler, P. C. (2024). Hamstring muscle injuries in athletics. The Physician and Sportsmedicine, 52(2), 103–114. https://doi.org/10.1080/00913847.2023.2188871
3. Yang, S., Cheng, J., Shang, J., Hang, C., Qi, J., Zhong, L., Rao, Q., He, L., Liu, C., Ding, L., Zhang, M., Chakrabarty, S., & Jiang, X. (2023). Stretchable surface electromyography electrode array patch for tendon location and muscle injury prevention. Nature Communications, 14(1), 6494. https://doi.org/10.1038/s41467-023-42149-x
4. Nieto Torrejón, L., Martínez-Serrano, A., Villalón, J. M., & Alcaraz, P. E. (2024). Economic impact of muscle injury rate and hamstring strain injuries in professional football clubs. Evidence from LaLiga. PLOS ONE, 19(6), e0301498. https://doi.org/10.1371/journal.pone.0301498
5. Wang, J., & Meng, H. (2023). Sport Fatigue Monitoring and Analyzing Through Multi-Source Sensors. International Journal of Distributed Systems and Technologies, 14(2), 1–11. https://doi.org/10.4018/ijdst.317941
6. Wu, J., Chen, Z., & Sun, L. (2025). System Integration of Multi-Source Wearable Sensors for Non-Invasive Blood Lactate Estimation: A Data Fusion Approach. Processes, 13(9), 2810. https://doi.org/10.3390/pr13092810

7. Isern-Kebschull, J., Mechó, S., Pedret, C., Pruna, R., Alomar, X., Kassarjian, A., Luna, A., Martínez, J., Tomas, X., & Rodas, G. (2024). Muscle healing in sports injuries: MRI findings and proposed classification based on a single institutional experience and clinical observation. Radiographics, 44(8), 230147. https://doi.org/https://doi.org/10.1148/rg.230147
8. Zhang, Q., Li, Y., Li, Y., Yang, X., & Abbasi, Q. H. (2022). Monitoring of neck activity for early warning of cervical spondylosis. Mathematical Biosciences and Engineering, 19(1), 792–811. https://doi.org/10.3934/mbe.2022036
9. Prys, M., Rosiński, Ł., Buryta, R., Radzimiński, Ł., Różewski, P., & Rejer, I. (2023). Integrating Machine Learning for Football Injury Prediction: A Concept for an Intelligent System. Procedia Computer Science, 225, 4139–4147. https://doi.org/10.1016/j.procs.2023.10.410
10. Dulfer, S. E., Gadella, M. C., Tamási, K., Absalom, A. R., Lange, F., Scholtens-Henzen, C. H. M., Faber, C., Wapstra, F. H., Groen, R. J. M., Sahinovic, M. M., Ulkatan, S., & Drost, G. (2023). Use of NEedle Versus suRFACE Recording Electrodes for Detection of Intraoperative Motor Warnings: A Non-Inferiority Trial. The NERFACE Study Part II. Journal of Clinical Medicine, 12(5), 1753. https://doi.org/10.3390/jcm12051753
11. Li, N., Zhou, R., Krishna, B., Pradhan, A., Lee, H., He, J., & Jiang, N. (2024). Non-invasive Techniques for Muscle Fatigue Monitoring: A Comprehensive Survey. ACM Computing Surveys, 56(9), 1–40. https://doi.org/10.1145/3648679
12. Al-Ayyad, M., Owida, H. A., De Fazio, R., Al-Naami, B., & Visconti, P. (2023). Electromyography Monitoring Systems in Rehabilitation: A Review of Clinical Applications, Wearable Devices and Signal Acquisition Methodologies. Electronics, 12(7), 1520. https://doi.org/10.3390/electronics12071520
13. Ackermans, L. L. G. C., Rabou, J., Basrai, M., Schweinlin, A., Bischoff, S. C., Cussenot, O., Cancel-Tassin, G., Renken, R. J., Gómez, E., Sánchez-González, P., Rainoldi, A., Boccia, G., Reisinger, K. W., Ten Bosch, J. A., & Blokhuis, T. J. (2022). Screening, diagnosis and monitoring of sarcopenia: When to use which tool? Clinical Nutrition ESPEN, 48, 36–44. https://doi.org/10.1016/j.clnesp.2022.01.027
14. Im, Y. J., Choe, Y., Lee, J., Lee, J., Do, J. G., & Kwon, J. (2025). Quantitative Muscle Ultrasound: A Non-Invasive Biomarker for Monitoring Duchenne Muscular Dystrophy. Muscle & Nerve, 72(4), 606–615. https://doi.org/10.1002/mus.28469
15. Xu, J., Tat, T., Yin, J., Ngo, D., Zhao, X., Wan, X., Che, Z., Chen, K., Harris, L., & Chen, J. (2023). A textile magnetoelastic patch for self-powered personalized muscle physiotherapy. Matter, 6(7), 2235–2247. https://doi.org/10.1016/j.matt.2023.06.008
16. Zhang, P., Deng, Z., Meng, Z., Li, H., Wang, J., & Wang, L. (2023). Pedestrian Inertial Positioning Method Based on Foot Quasi-Zero Velocity Observation Under Multiple Motion Modes. IEEE Internet of Things Journal, 10(20), 18438–18447. https://doi.org/10.1109/jiot.2023.3280505
17. Zheng, Y., Lanovaz, Joel L., Johnston, J. (JD), & Kontulainen, S. A. (2024). Precision errors and monitoring time interval in pediatric muscle imaging and neuromuscular performance assessment. Journal of Musculoskeletal & Neuronal Interactions, 24(1), 1–11.
18. Tani, Y., Sato, T., Taniguchi, S., Masayuki, I., Paku, M., Adachi, T., Ando, M., Kohara, N., & Kimura, J. (2022). Threshold-based monitoring of compound muscle action potentials for percutaneous pedicle screw placement in the lumbosacral spine: Can we rely on stimulation of the uninsulated screw to provide a valid safety warning? Spine, 47(14), 1003–1010. https://doi.org/10.1097/BRS.0000000000004263
19. Murphy, G. S., & Brull, S. J. (2022). Quantitative Neuromuscular Monitoring and Postoperative Outcomes: A Narrative Review. Anesthesiology, 136(2), 345–361. https://doi.org/10.1097/aln.0000000000004044
20. Liu, L., Wang, X., Wang, Y., Wang, M., Ma, Y., & Li, J. (2024). The value of quantitative muscle ultrasound in monitoring muscle and fascia inflammatory activity in juvenile dermatomyositis patients. Quantitative Imaging in Medicine and Surgery, 14(12), 8601–8613. https://doi.org/10.21037/qims-24-1035
21. Xie, S., Liu, W., Duan, H., Chen, D., & Wan, Y. (2023). A Digital Twin-based Framework of Motion Control and State Monitoring for Pneumatic Muscle. Recent Patents on Mechanical Engineering, 16(3), 203–213. https://doi.org/10.2174/2212797616666230612152528
22. Khanal, S. R., Paulino, D., Sampaio, J., Barroso, J., Reis, A., & Filipe, V. (2022). A review on computer vision technology for physical exercise monitoring. Algorithms, 15(12), 444. https://doi.org/https://doi.org/10.3390/a15120444
23. Tang, H., Li, Y., Chen, B., Chen, X., Han, Y., Guo, M., Xia, H., Song, R., Zhang, X., & Zhou, J. (2022). In Situ Forming Epidermal Bioelectronics for Daily Monitoring and Comprehensive Exercise. ACS Nano, 16(11), 17931–17947. https://doi.org/10.1021/acsnano.2c03414
24. Omarov, B., Omarov, N., Mamutov, Q., Kissebayev, Z., Anarbayev, A., Tastanov, A., & Yessirkepov, Z. (2024). Examination of the Augmented Reality Exercise Monitoring System as an Adjunct Tool for Prospective Teacher Trainers. Retos, 58, 85–94. https://doi.org/10.47197/retos.v58.105030
25. Alvarez, J. T., Gerez, L. F., Araromi, O. A., Hunter, J. G., Choe, D. K., Payne, C. J., Wood, R. J., & Walsh, C. J. (2022). Towards Soft Wearable Strain Sensors for Muscle Activity Monitoring. IEEE Transactions on Neural Systems and Rehabilitation Engineering, 30, 2198–2206. https://doi.org/10.1109/tnsre.2022.3196501
26. Shang, M., Dedeyne, L., Dupont, J., Vercauteren, L., Amini, N., Lapauw, L., Gielen, E., Verschueren, S., Varon, C., De Raedt, W., & Vanrumste, B. (2024). Otago Exercises Monitoring for Older Adults by a Single IMU and Hierarchical Machine Learning Models. IEEE Transactions on Neural Systems and Rehabilitation Engineering, 32, 462–471. https://doi.org/10.1109/tnsre.2024.3355299
27. Laganà, F., Pratticò, D., Angiulli, G., Oliva, G., Pullano, S. A., Versaci, M., & La Foresta, F. (2024). Development of an Integrated System of sEMG Signal Acquisition, Processing, and Analysis with AI Techniques. Signals, 5(3), 476–493. https://doi.org/10.3390/signals5030025
28. Zhu, B., Zhang, D., Chu, Y., Gu, Y., & Zhao, X. (2022). SeNic: An Open Source Dataset for sEMG-Based Gesture Recognition in Non-Ideal Conditions. IEEE Transactions on Neural Systems and Rehabilitation Engineering, 30, 1252–1260. https://doi.org/10.1109/tnsre.2022.3173708
29. Shin, J., Miah, A. S. M., Konnai, S., Takahashi, I., & Hirooka, K. (2024). Hand gesture recognition using sEMG signals with a multi-stream time-varying feature enhancement approach. Scientific Reports, 14(1), 22061. https://doi.org/10.1038/s41598-024-72996-7
30. Miah, A. S. M., Shin, J., & Hasan, Md. A. M. (2024). Effective features extraction and selection for hand gesture recognition using sEMG signal. Multimedia Tools and Applications, 83(37), 85169–85193. https://doi.org/10.1007/s11042-024-19468-2

DOI: 10.3844/ajbbsp.2026.22.03.033

31. Shin, S., Li, Z., & Halilaj, E. (2023). Markerless Motion Tracking With Noisy Video and IMU Data. IEEE Transactions on Biomedical Engineering, 70(11), 3082–3092. https://doi.org/10.1109/tbme.2023.3275775
32. Xuan, L., He, X., Yi, Y., Shen, A., Yang, X., Dong, J., & Dong, S. (2024). Research on IMU-Based Motion Attitude Acquisition and Motion Recognition. IEEE Sensors Journal, 24(13), 20786–20793. https://doi.org/10.1109/jsen.2024.3394903
33. Zhang, S., Gao, H., & Yang, F. (2025). Research on Wearable Devices for Pedestrian Navigation Based on the Informer Model Zero-Velocity Update Architecture. Sensors, 25(8), 2587. https://doi.org/10.3390/s25082587
34. Zhang, W., Ju, L., Jia, H., Ding, X., & Feng, Y. (2023). Semiring-Optic-Fiber (SROF) Sensor-Based Abnormal Gait Recognition via Monitoring Muscle Activation. IEEE Sensors Journal, 23(17), 19307–19317. https://doi.org/10.1109/jsen.2023.3292923
35. Marino, A., Pacchierotti, C., & Giordano, P. R. (2024). Input State Stability of Gated Graph Neural Networks. IEEE Transactions on Control of Network Systems, 11(4), 2052–2063. https://doi.org/10.1109/tcns.2024.3372710
36. Xu, R., Luo, F., Zhu, Z., Li, M., & Chen, B. (2022). Flexible Wide-Range Triboelectric Sensor for Physiological Signal Monitoring and Human Motion Recognition. ACS Applied Electronic Materials, 4(8), 4051–4060. https://doi.org/10.1021/acsaelm.2c00681